Pharmacologic Stabilization of Retromer Rescues Endosomal Pathology Induced by Defects in the Alzheimer's gene *SORL1*

Swati Mishra[1,2*], Allison Knupp[1,2*] , Chizuru Kinoshita[1,2], Refugio Martinez[1,2], Panos Theofilas[3], and Jessica E. Young[1,2,#]

[1]Department of Laboratory Medicine and Pathology, University of Washington Seattle WA, 98195, USA

[2]Institute for Stem Cell and Regenerative Medicine, University of Washington Seattle WA, 98195, USA

[3]Memory and Aging Center, Department of Neurology, University of California, San Francisco, San Francisco, CA 94158

*Equal contributions

[#]Correspondence: jeyoung@uw.edu

Abstract:

Defects in the Sortilin-related receptor 1 gene, *SORL1*, are highly pathogenic in Alzheimer's disease (AD), on par with other causal AD genes. *SORL1* is a key regulator of endosomal trafficking in neurons, and loss of *SORL1* function disrupts trafficking pathways that are vital for neuronal health. *SORL1* has been found to interact with retromer, a protein complex that is a 'master conductor' of endosomal trafficking. Here we rely on retromer pharmacological chaperones that stabilize retromer *in vitro*, and thus enhance retromer function in cells. to test the hypothesis that they will correct AD-associated neuronal pathologies. We used an isogenic series of human induced pluripotent stem cell (hiPSCs) lines either deficient in *SORL1* expression (*SORL1* KO or $SORL1^{+/-}$) or harboring one copy of a missense variant linked to increased risk for AD ($SORL1^{Var}$). We treated neurons derived from these hiPSCs with the established retromer chaperone, TPT-260, and tested whether they corrected indicators of AD's defining endosomal, amyloid, and Tau pathologies. We observed that TPT-260 treatment was able to correct all these pathological indicators; however, the degree of rescue of some of the phenotypes was dependent on whether the neurons harbor at least one functional copy of *SORL1* or whether they are fully deficient. More than just validating that *SORL1*-retromer acts as a functional trafficking unit in neurons, our work sheds new light on how *SORL1*-retromer is linked to AD's cardinal pathologies and illuminates how this pathway can be therapeutically harnessed.

Introduction:

Alzheimer's disease (AD) is a devastating neurodegenerative disorder that affects a growing population of older adults. There are currently very few medications that even temporarily alleviate symptoms of AD and no treatment that effectively modifies the course of the disorder for more than several months. Drugs in current clinical trials focus on targeting amyloid beta (Aβ), the main component of senile plaques, which are a hallmark AD neuropathology. However, genetic studies, including large genome-wide association studies, have identified dozens of AD risk loci that map to various cellular processes, including endo-lysosomal trafficking (Karch and Goate, 2015). Abnormal endosomes and lysosomes in human brains have long been identified as a pathologic hallmark of AD since the first description of the disorder and subsequently by elegant microscopy studies several decades ago (Cataldo et al., 1996; Cataldo et al., 2004; Cataldo et al., 2000). More recent cell biological studies have particularly implicated deficiencies in retromer-related endosomal trafficking and recycling as a mechanism that leads to this pathology that contributes to the neuropathologic hallmarks of AD: Aβ and phosphorylated microtubule- and actin-associated protein Tau (Knupp et al., 2020; Simoes et al., 2021; Young et al., 2018). Central to this mechanism is the gene *SORL1*, an endosomal sorting receptor that has emerged as a highly pathogenic AD gene (Scheltens et al., 2021). Missense mutations in the gene, including G511R, Y141C and E270K, have been identified as damaging variants that can contribute to AD pathogenesis through loss of function of *SORL1* (Pottier et al., 2012; Vardarajan et al., 2014).

The *SORL1* gene encodes the sorting receptor SORLA, which functions in retromer-dependent trafficking of cargo through the endo-lysosomal network. SORLA engages with the multi-protein sorting complex retromer as an adaptor protein for multiple cargo, including APP, Aβ peptides, neurotrophin receptors, and glutamate receptors (Fjorback et al., 2012; Mishra et al., 2022; Simoes et al., 2021). *SORL1* KO neurons derived from hiPSCs have endosomal traffic jams marked by enlarged early endosomes, mislocalized neuronal cargo, impairments in endosomal degradation and recycling (Hung et al., 2021; Knupp et al., 2020; Mishra et al., 2022). Both endosomal recycling and degradation pathways in neurons are enhanced in a model where *SORL1* is overexpressed (Mishra et al., 2022), suggesting that increasing *SORL1* expression in neurons may be beneficial in AD. However, *SORL1* is a difficult therapeutic target due to its size and complexity: the gene contains 48 exons and large intronic regions and the protein itself is 2214 amino acids (Rogaeva et al., 2007).

Alternatively, enhancing endosomal trafficking via targeting the retromer complex, which is intimately associated with *SORL1*, may be a feasible therapeutic strategy. Small molecule

pharmacologic chaperones that stabilize the cargo recognition core of retromer *in vitro* have been developed and have been shown to reduce amyloidogenic processing of APP in models of AD and increase the flow of SORLA through endosomes (Mecozzi et al., 2014). Both retromer and *SORL1* are decreased in AD brains and retromer deficient mice show synaptic dysfunction and memory impairment. *SORL1* directly binds retromer through its interaction with the retromer subunit VPS26 (Bhalla et al., 2012; Fjorback et al., 2012; Small et al., 2005)

In this study, we used our previously published *SORL1* deficient hiPSC cell lines (*SORL1* KO) (Knupp et al., 2020) as well as new lines that we engineered to have loss of *SORL1* on one allele ($SORL1^{+/-}$) or to have one copy of an AD-associated *SORL1* variant in the VPS10 domain ($SORL1^{Var}$) to investigate whether enhancing retromer-related trafficking can improve endosomal phenotypes. We report that in hiPSC-derived neurons from $SORL1^{+/-}$ and $SORL1^{Var}$ lines, we observe enlarged early endosomes and increased Aβ secretion. We show that treatment with TPT-260 (also known as R55), a pharmacologic chaperone that stabilizes retromer in vitro (Mecozzi et al., 2014), rescues these phenotypes. We also report than TPT-260 can improve endo-lysosomal trafficking and endosomal recycling in *SORL1* deficient hiPSC-derived neurons. In addition to rescuing endo-lysosomal phenotypes, TPT-260 lowers phosphorylated Tau (p-Tau), suggesting that this pathway can converge on multiple cellular phenotypes in AD. Interestingly, some of the phenotypes we studied had differential rescue effects after TPT-260 treatment based on whether they were partially deficient ($SORL1^{+/-}$) or fully deficient (*SORL1* KO) for *SORL1*. As loss of one copy of *SORL1* has been shown to be causative for AD, our data suggest that the *SORL1*-retromer axis is important for future therapeutic development in AD.

Results:

$SORL1^{+/-}$ and $SORL1^{Var}$ hiPSC-derived neurons have enlarged early endosomes and increased Aβ secretion.

Using CRISPR/Cas9 genome editing, we generated isogenic stem cell lines containing either heterozygous AD-associated variants in the VPS10 domain: E270K, Y141C, and G511R ($SORL1^{Var}$) or heterozygous loss of *SORL1* ($SORL1^{+/-}$) **(Supplemental Figure 1).** Western blot analysis revealed that $SORL1^{Var}$ neurons do not have a loss of SORLA protein expression as these missense variants do not introduce a frame-shift **(Supplemental Figure 1**) or destabilize the protein enough for it to be degraded. However, $SORL1^{+/-}$ neurons have reduced *SORL1* expression compared with isogenic WT controls (**Supplemental Figure 1**).

Enlarged early endosomes have become one of the defining cytopathologies of AD, indicative of endosomal “traffic jams” (Small et al., 2017). We and others have previously

observed enlarged early endosomes in homozygous *SORL1* KO hiPSC-derived neurons (Hung et al., 2021; Knupp et al., 2020). We hypothesized that *SORL1*$^{+/-}$ and *SORL1*^{Var} neurons would similarly contain enlarged early endosomes, although we predicted that due to the single copy of WT *SORL1*, the phenotype could be more subtle. We immunostained *SORL1* KO, *SORL1*$^{+/-}$, and *SORL1*^{Var} neurons with EEA1 to mark early endosomes, imaged cells using confocal microscopy, and quantified early endosome size using Cell Profiler as we have previously described (Knupp et al., 2020). We observed a significant increase in endosome size in *SORL1*^{Var}, *SORL1*$^{+/-}$, and *SORL1*KO neurons compared to isogenic WT controls (**Figure 1 A-B**). Interestingly, endosomes in neurons with one copy of WT *SORL1* (*SORL1*^{Var} and *SORL1*$^{+/-}$) were not as enlarged as in cells with the full *SORL1* KO (**Figure 1B**). These data indicate that harboring one copy of an AD-associated variant in *SORL1* is sufficient to induce early endosome enlargement in cortical neurons and that loss of *SORL1* expression can contribute to endosome enlargement in a gene dose dependent manner.

Loss of *SORL1* contributes to increased APP processing because SORLA is an adaptor protein for retromer trafficking of APP and when SORLA is absent, APP is stuck in early and recycling endosomes where it can be more readily processed to Aβ (Das et al., 2016; Knupp et al., 2020; Mishra et al., 2022; Tan and Gleeson, 2019; Toh et al., 2018). We have previously reported increased secreted Aβ in *SORL1* KO neurons (Knupp et al., 2020). In this study, we also observe an increase in secreted Aβ peptides in *SORL1*$^{+/-}$ and *SORL1*^{Var} neurons as measured by ELISA assays. In agreement with these neurons having at least one functional copy of *SORL1*, compared to a full *SORL1* KO, the increase in secreted Aβ peptides is not as pronounced in *SORL1*$^{+/-}$ or *SORL1*^{Var} neurons (**Figure 1C-D**).

TPT-260 treatment reduces endosome size, secreted Aβ levels and pTau levels in *SORL1* KO, *SORL1*$^{+/-}$, and *SORL1*^{Var} neurons.

These data and our previously published work (Knupp et al., 2020; Mishra et al., 2022) strongly suggest that alterations in SORL1 impact the endo-lysosomal network and result in pathological processes involved in AD. Therefore, we tested whether enhancing endo-lysosomal function via small molecules could rescue pathological phenotypes. We chose to study the effects of a pharmacological chaperone, TPT-260 (also called R55), which stabilizes and enhances retromer *in vitro* by binding the VPS35-VPS26-VPS29 trimer in the cargo-recognition core of the multi-subunit retromer complex (Mecozzi et al., 2014). Previously, we have shown that a similar molecule, TPT-172 (also known as R33), was effective at reducing Aβ and pTau levels in hiPSC-derived neurons from AD patients and controls (Young et al., 2018). We first tested whether TPT-

260 would have an effect on early endosome size as this is one of the earliest cytopathological changes in AD (Cataldo et al., 2000) and is indicative of endosomal traffic jams that impact endo-lysosomal degradation and endosomal recycling (Mishra et al., 2022). In *SORL1* KO, *SORL1*$^{+/-}$, and *SORL1*^{Var} neurons, treatment with TPT-260 reduced endosome size compared with vehicle (DMSO) treated controls (**Figure 2A-B**). We did not observe any changes in EEA1 puncta size in WT neurons treated with TPT-260, indicating that the retromer chaperone does not alter the size of endosomes that are not enlarged. In *SORL1*$^{+/-}$ and *SORL1*^{Var} neurons treated with TPT-260, endosome size was significantly reduced and was not significantly different than in WT neurons treated with TPT-260. Interestingly, while endosome size was also reduced in neurons with full *SORL1* KO, endosome size in these neurons was not reduced to WT levels, indicating that without at least one copy of *SORL1*, this phenotype cannot be fully resolved.

We next tested whether enhancing retromer function could reduce Aβ peptides in *SORL1* KO, *SORL1*$^{+/-}$ or *SORL1*^{Var} neurons. We treated hiPSC-derived neurons from *SORL1* KO, *SORL1*$^{+/-}$, and *SORL1*^{Var} cell lines with 15μM TPT-260 for 72 hours. This treatment is similar to previous studies in neuronal cells (Young et al., 2018), is not toxic to neuronal cultures, and significantly increases VPS35 protein levels (**Supplemental Figure 3**). From these cultures we measured the amount of Aβ peptides secreted into the media using an ELISA assay. In all cell lines we observed decreased secreted Aβ peptides with TPT-260 treatment; however, in neurons with full *SORL1* KO, Aβ 1-40 levels, while reduced, were still significantly higher than in the other conditions **(Figure 2C)**. Interestingly, Aβ 1-42 levels were not changed with TPT-260 treatment in *SORL1* KO neurons although they were reduced to WT levels in all cell lines with one copy of *SORL1* (**Figure 2D).**

Accumulation of phosphorylated Tau (pTau) protein is a significant neuropathological hallmark in AD and retromer chaperones have been reported to decrease pTau levels in both hiPSC-neurons and mouse models of AD and tauopathy (Li et al., 2020; Young et al., 2018). Interestingly, retromer chaperones decrease pTau independently of Aβ and APP (Young et al., 2018). In our hiPSC-neuronal model, we did not detect significant changes in pTau in neurons *SORL1*KO or in any of our *SORL1*^{Var} neurons (**Supplemental Figure 2**), although in other studies where *SORL1* KO hiPSC-derived neurons are differentiated using the expression of the transcription factor NGN2, loss of *SORL1* does lead to increased phospho-Tau (Tracy Young-Pearse, personal communication). Despite this, when we treated all genotypes of neurons with TPT-260, we

observed that treatment did significantly reduce pTau at several epitopes in all cell lines and there was no difference in the level of reduction relative to *SORL1* gene dose (**Figure 2 E-G**).

TPT-260 treatment fully reduces localization of VPS35 from early endosomes, but only partially rescues localization of APP from early endosomes in *SORL1* KO neurons.

We previously demonstrated that in *SORL1* KO neurons, both VPS35, a core component of retromer, and APP showed increased localization in early endosomes (Knupp et al., 2020; Mishra et al., 2022). We examined whether TPT-260 treatment could affect this mis-localization. Indeed, treatment with TPT-260 completely rescued VPS35 accumulation in early endosomes in *SORL1* KO neurons, indicating that this treatment was able to mobilize retromer away from early endosomes (**Figure 3A-B**). When we analyzed APP localization upon TPT-260 treatment, we observed that there was still significantly more APP colocalization with early endosomes than in WT cells treated with TPT-260 (**Figure 3C-D**). This observation is consistent with *SORL1* being a main adaptor protein for APP and retromer via VPS26 (Fjorback et al., 2012). We next examined APP/EEA1 colocalization in *SORL1*$^{+/-}$ neurons treated with TPT-260 and here we show that treatment returns APP/EEA1 colocalization to levels similar to WT neurons (**Figure 3D**). This finding could explain why the reduction of Aβ peptides in TPT-260 treated *SORL1* KO neurons is not as significant as in neurons with at least one WT copy of *SORL1*; in neurons without any copies of *SORL1*, APP is still largely localized to early endosomes where it can be processed to Aβ.

Impaired endosomal recycling and lysosomal degradation in *SORL1* KO neurons are improved by pharmacologic stabilization of retromer

In *SORL1* KO neurons, endosomal traffic jams impede cargo traffic to late endosomes and lysosomes as well as to the cell surface recycling pathway (Mishra et al., 2022). *SORL1* has been shown to function in both pathways by shuttling Aβ to lysosomes (Caglayan et al., 2014) as well as promoting the recycling of APP and glutamate receptors to the cell surface (Mishra et al., 2022). The latter function has been shown to involve a neuron-specific subunit of retromer, VPS26b (Simoes et al., 2021). We analyzed lysosomal degradation in WT and *SORL1* KO neurons treated with TPT-260 or vehicle (DMSO) using the DQ-Red-BSA assay. In this assay, cells show red fluorescence only upon degradation of DQ-BSA, which largely occurs in the lysosomes (Marwaha and Sharma, 2017). We observed a significant reduction in DQ-Red-BSA fluorescence at 24 hours in DMSO treated *SORL1* KO neurons (**Figure 4B**), consistent with our previous observations (Mishra et al., 2022). In TPT-260 treated neurons, we document a complete

rescue of this phenotype (**Figure 4B**) suggesting that retromer stabilization can promote this pathway, even in the absence of *SORL1*. To test endosomal recycling, we utilized the transferrin recycling assay, a classic measure of both fast and slow endosomal recycling(Ouellette and Carabeo, 2010; Sonnichsen et al., 2000). This assay utilizes fluorescently labeled transferrin and quantifies loss of fluorescence over time as transferrin is internalized and subsequently recycled from the cells. In DMSO conditions, we observed a significant reduction in transferrin recycling in *SORL1* KO neurons, consistent with our previous observations (Mishra et al., 2022) (**Figure 4D**). Interestingly, in TPT-260 conditions, we noted a partial rescue of transferrin recycling in *SORL1* KO neurons, however even with TPT-260 treatment, recycling was still significantly slower that in WT neurons (+ or – TPT-260) at later time points in the assay (**Figure 4D**). These data suggest that enhancing retromer can promote endosomal recycling but at least one functional copy of *SORL1* is needed to recycle cargo as efficiently as in WT neurons.

Taken together, our data suggest that enhancing retromer promotes lysosomal degradation as well as endosomal recycling. However, in neurons, fully efficient endosomal recycling seems to require *SORL1*.

Discussion

When considering the development of novel therapeutics for Alzheimer's disease, it is critical to examine biologically relevant pathways such as protein trafficking through the endo-lysosomal network in neurons. In particular, trafficking of APP directly affects its processing into Aβ. Furthermore, indicators of endosomal dysfunction, such as enlarged or swollen endosomes, are early cytopathological phenotypes in AD, evident before substantial accumulation of other neuropathologic hallmarks (Cataldo et al., 2000) and thus a potentially attractive therapeutic readout. In order to more fully explore this concept in human neurons, we used previously published and newly generated hiPSC lines that are either deficient in *SORL1* expression (*SORL1* KO or *SORL1*$^{+/-}$) or that harbor AD-associated coding variants in the VPS10 domain of the protein (*SORL1*^{Var}) and treated neurons differentiated from these hiPSCs with TPT-260, a small molecule chaperone that stabilized retromer and enhances its function (Mecozzi et al., 2014).

We and others have previously reported that that heterozygous and homozygous loss of *SORL1* results in increased secretion of Aβ and enlarged early endosomes(Hung et al., 2021; Knupp et al., 2020). In this study, we also observed increases in secreted Aβ and enlarged endosomes in our *SORL1*^{Var} lines (**Figure 1**). Both secreted Aβ and enlarged early endosome phenotypes seem to be dependent on whether or not a WT allele of *SORL1* is present, which

aligns with previous reports(Dodson et al., 2008; Hung et al., 2021). These data are also consistent with indications that *SORL1* haploinsufficiency is causative for AD (Holstege et al., 2017; Scheltens et al., 2021), and suggests that certain AD-associated variants may result in loss of important *SORL1* functions and lead to AD.

The *SORL1* protein, SORLA, is the main adaptor protein for retromer-dependent trafficking of APP and Aβ peptides (Andersen et al., 2005; Caglayan et al., 2014; Fjorback et al., 2012). Therefore, in *SORL1* KO neurons, we expected that there would be a smaller effect on Aβ secretion after treatment with TPT-260 than in cell lines with one functional copy of *SORL1*, and this is what we observed. *SORL1* KO neurons show only slightly reduced Aβ40 secretion, and no change in Aβ42 secretion with TPT-260 treatment (**Figure 2).** However, in the more clinically relevant scenario of either *SORL1*$^{+/-}$or *SORL1*^{Var} in which cells still have one wild-type copy of *SORL1*), TPT-260 treatment reduced both Aβ40 and Aβ42 to WT levels.

In this study we did not observe a significant increase in pTau in either our *SORL1* deficient cell lines or our *SORL1*^{Var} lines; however, this observation may also depend on the method of neuronal differentiation. It is still worth noting that in this model TPT-260 treatment lowers phospho-Tau levels on multiple epitopes in this model. Our data here (**Figure 2**) provide an independent corroboration of previous work (Young et al., 2018) and also supports what has been seen in tauopathy models (Li et al., 2020; Young et al., 2018). Tau clearance by endo-lysosomal trafficking is an important aspect of maintaining Tau homeostasis and efficient clearance of phosphorylated Tau is an important step in preventing pathological aggregation (Tang et al., 2019). Our results showing that TPT-260 lowers multiple forms of phospho-Tau also highlight the potential therapeutic relevance of retromer functional enhancement.

The early endosome is the sorting hub for cargo in the endo-lysosomal network, and enlarged early endosomes are indicative of traffic jams (Small et al., 2017). Importantly, enlarged early endosomes are a very early cellular pathology in AD, arising prior to widespread Aβ and pTau pathology (Cataldo et al., 2000). Enlarged early endosomes are also apparent in familial AD cell lines, where altered APP processing is a main disease driver. In these conditions, reducing amyloidogenic processing by treatment with a β-secretase inhibitor (BACEi) was able to rescue endosome enlargement (Kwart et al., 2019). In contrast, enlarged endosomes due to loss of *SORL1* expression were not rescued by treatment with BACEi (Knupp et al., 2020) but were rescued by total reduction of APP using anti-sense oligos (Hung et al., 2021), which suggests that reducing total endosomal cargo may be beneficial. In this study, we tested whether TPT-260 treatment would have an effect on enlarged endosomes observed in *SORL1* KO, *SORL1*$^{+/-}$, and

SORL1^{Var} neurons. Interestingly, TPT-260 treatment reduced endosome size in all genotypes, however only in neurons with at least one copy of *SORL1* were endosome sizes fully reduced to WT levels. Importantly for therapeutic implications, the retromer chaperone does not appear to affect endosome size in the WT cell lines at the concentrations we tested. Together this set of data indicates endosome enlargement in *SORL1* deficient or variant cells is due to loss of *SORL1* function, which impacts the flow of proteins through the endosomal network. Strategies that reduce the total amount of cargo within early endosomes, such as reduction of total APP or enhancement of retromer function, may thus help to alleviate endosome enlargement.

We examined the localization of the retromer core protein VPS35 and the canonical *SORL1*-retromer cargo, APP. We previously reported that both APP and VPS35 are increased in early endosomes in *SORL1* KO neurons (Knupp et al., 2020; Mishra et al., 2022). TPT-260 treatment reduced the localization of VPS35 in early endosomes to WT levels in *SORL1* KO cells, showing that this treatment is sufficient to mobilize retromer in these cells (**Figure 3**). However, because SORLA is a main adaptor protein between retromer and APP, it is possible that in full *SORL1* KO cells, there might not be a large change in APP localization with TPT-260 treatment. Indeed, in neurons treated with TPT-260, there is still significantly more APP localized in early endosomes than in TPT-260 treated WT neurons (**Figure 3**). In neurons with at least one copy of *SORL1* (*SORL1*$^{+/-}$) neurons, TPT-260 treatment APP co-localization with early endosomes is similar to WT APP/EEA1 co-localization (**Figure 3**). Because amyloidogenic cleavage of APP occurs in the early endosomes, this finding could explain why Aβ levels in *SORL1*$^{+/-}$ neurons are completely rescued with TPT-260 treatment, while Aβ levels in *SORL1* KO neurons are not.

Endosomal traffic jams impact multiple arms of the endo-lysosomal network. Cargo stuck in early endosomes is less likely to transit to lysosomes for degradation or to be recycled back to the cell surface, both essential pathways for efficient neuronal function (Mishra et al., 2022). We have previously shown that *SORL1* KO neurons show deficiencies in both trafficking to lysosomes as well as cell surface recycling. Here we tested whether TPT-260 treatment could rescue these deficiencies. We show using a DQ-Red-BSA assay that TPT-260 enhances trafficking to lysosomes in *SORL1* KO cells, bringing this function to WT levels (**Figure 4**). On the other hand, we observed only a partial rescue of transferrin recycling in full *SORL1* KO cells (**Figure 4**). In neurons, *SORL1* interacts with a neuron-specific isoform of the retromer complex, VPS26b, to recycle cargo such as glutamate receptors (Simoes et al., 2021). Our data suggest that in full *SORL1* KO, retromer enhancement is insufficient to fully rescue this phenotype.

Altogether, our work shows that treatment with a small molecule that stabilizes retromer *in vitro* and enhances retromer-related trafficking can reduce important cellular (swollen

endosomes) and neuropathologic (Aβ and pTau) phenotypes in human AD neuronal models. Furthermore, we dissect the role of *SORL1*-retromer in endosomal recycling and endo-lysosomal trafficking, functions essential to efficient neuronal function. Using a small molecule retromer chaperone, we broadly show that enhancement of this pathway can fully or partially rescue deficits induced by loss of *SORL1*. Although there is one report of a full loss of *SORL1* (Le Guennec et al., 2018), most patients where *SORL1* is a main risk factor for disease development still maintain at least one functional copy of *SORL1*. Our work provides evidence that the *SORL1*-retromer pathway is a strong candidate for therapeutic intervention in AD. Importantly, this study builds on previous work that has used these chaperones in animals and human cells, suggesting that studies such as this could represent an important pre-clinical step in identifying new therapeutic molecules for AD.

Limitations to our study: Our study has certain limitations. First, we focused on variants present in the VPS10 domain of *SORL1* (Andersen et al., 2016; Pottier et al., 2012; Vardarajan et al., 2014). Some of these variants have been found in control subjects (Holstege et al., 2017), thus there are certainly other factors in various human genetic backgrounds that need to be considered. We engineered these variants in our well-characterized, male, hiPSC line (Knupp et al., 2020; Young et al., 2015). The genetic background of this line also harbors one copy of APOE ε4 and common variants in *SORL1* associated with increased AD risk in candidate-gene based studies (Levy et al., 2007; Rogaeva et al., 2007). Thus, we cannot rule out the contribution of these other genomic variants to our phenotypes. However, these are common variants, similar to what may predispose many humans to late onset AD development. Rescue of these cellular phenotypes using retromer-enhancing drugs is still an important observation that may be relevant to both earlier and later-onset forms of AD. Finally, our study is focused on neuronal cells. We recognize the importance of endosomal trafficking and *SORL1*-retromer related pathways in glia and other cell types relevant to the pathogenesis and/or progression of AD. Future studies will benefit from analyzing endo-lysosomal phenotypes in multiple CNS cell types.

Method details

Experimental model and subject details

Cell lines

CRISPR/Cas9 Genome Editing

All genome editing was completed in the previously published and characterized CV background human induced pluripotent stem cell line(Young et al., 2015), which is male with an APOE e3/e4 genotype(Levy et al., 2007). Genome editing was performed according to published protocols (Young et al., 2018). Briefly, the Zhang Lab CRISPR Design website (crispr.mit.edu) was used to generate guide RNAs (gRNAs) with minimal off-target effects. gRNAs were cloned into the px458 vector that also expresses GFP and the Cas-9 nuclease. hiPSCs were electroporated with plasmids, sorted by flow cytometry for GFP expression, and plated at a clonal density of ~1x10^4 cells per 10cm plate. After approximately two weeks of growth, colonies were picked and split into identical sets. One set was analyzed by Sanger sequencing and one set was expanded to generate isogenic cell lines. A total of 8 previously unpublished clones were chosen for experiments contained in this publication: 2 WT clones, 2 clones containing the heterozygous *SORL1* E270K variant (**Supplemental Figure 1A**), 1 clone containing the heterozygous *SORL1* Y141C variant (**Supplemental Figure 1B**), 2 clones containing the heterozygous *SORL1* G511R variant (**Supplemental Figure 1C**), and 1 clone containing a deletion resulting in a heterozygous *SORL1* KO (*SORL1*$^{+/-}$) (**Supplemental Figure 1D-F**). Also included in this publication are four previously published clones including 2 WT clones and 2 homozygous *SORL1* KO clones (*SORL1* KO)(Knupp et al., 2020; Mishra et al., 2022). All clones were shown to have normal karyotypes and verified to be free of mycoplasma (MycoAlert).

CRISPR/Cas9 gRNA, ssODN, and Primer Sequences

The CRISPR/Cas9 reagents used to generate the E270K cell lines are the same as what was used to generated the previously published *SORL1* KO hiPSC lines(Knupp et al., 2020). For the *SORL1* KO lines, clones were chosen that incorporated indels rather than the ssODN sequence.

E270K gRNA: ATTGAACGACATGAACCCTC

E270KssODN:

GGGAATTGATCCCTATGACAAACCAAATACCATCTACATTGAACGACATGAACCCTCTGGC

TACTCCACGTCTTCCGAAGTACAGATTTCTTCCAGTCCCGGGAAAACCAGGAAG

E270K Forward primer:ctctatcctgagtcaaggagtaac

E270K Reverse primer: ccttccaattcctgtgtatgc

PCR amplifies 458 bp sequence

Y141C gRNA: GTACGTGTCTTACGACTA

Y141C ssODN:

GAAAGATCTTTCTGCCAGTTTCTCACCAACTCTTTCTTTTTCATCTCCTTTTCTCTGTATTCC

AGGTGTACGTGTCTTACGACTGTGGAAAATCATTCAAGAAAATTTCAGACAAGTTAAACTTT
GGCTTGGGAAATAGGAGTGAAGCTG
Y141C Forward primer: gtggcaggtgcctgtaatcc
Y141C Reverse primer: cacagagagcgccatctcc
PCR amplifies 445 bp sequence

G511R gRNA: CTCTTGCATTTTAGGCTCAG
G511R ssODN:
CTGACATATTCTTGAAATTAAAAATAATTATTTCTCTTGCATTTTAGGCTCAGTGCGAAAGAA
CTTGGCTAGCAAGACAAACGTGTACATCTCTAGCAGTGCTGGAGCCAGGTGGCG
G511R Forward primer: cgccactggtaagtgtgcttgc
G511R Reverse primer: ctggcattactggtctctgccatg
PCR amplifies 413 bp sequence

Method details

Differentiation of neurons from human induced pluripotent stem cells (hiPSCs)

hiPSCs were cultured and differentiated into neurons using previously published methods(Knupp et al., 2020; Mishra et al., 2022; Rose et al., 2018). Briefly, cortical neurons were differentiated from hiPSCs using the dual-SMAD inhibition technique. hiPSCs were plated on 1:20 Matrigel-coated (Growth factor reduced basement membrane matrix; # 356231; Corning) 6-well plates at a density of 3.5 million cells per well. Cells were fed with Basal Neural Maintenance Media (BNMM) (1:1 DMEM/F12 (#11039047 Life Technologies) + glutamine media/neurobasal media (#21103049, Gibco), 0.5% N2 supplement (# 17502-048; Thermo Fisher Scientific,) 1% B27 supplement (# 17504-044; Thermo Fisher Scientific), 0.5% GlutaMax (# 35050061; Thermo Fisher Scientific), 0.5% insulin-transferrin-selenium (#41400045; Thermo Fisher Scientific), 0.5% NEAA (# 11140050; Thermo Fisher Scientific), 0.2% β-mercaptoethanol (#21985023, Life Technologies)) supplemented with 10 ⌈M SB-431542 and 0.5 ⌈M LDN-193189 (#1062443, Biogems) for seven days. On day 8, cells were incubated with Versene (#15640066, Gibco), dissociated with cell scrapers, and passaged 1:3. From days 9-13, cells were fed daily with BNMM containing no supplements. On day 13, media was switched to BNMM containing 20 ng/mL FGF (R&D Systems, Minneapolis, MN). On day 16, cells were passaged 1:3. Cells were fed daily until approximately day 23, when cells were FACS sorted to enrich a stable population of CD184/CD24 (#557145/561646 BD Pharmingen) positive, CD44/CD271 (#555479/557196 BD Pharmingen)

negative neural progenitor cells(Yuan et al., 2011). After sorting, cells were expanded for cortical neuronal differentiation. Neural progenitor cells were plated on Matrigel at a density of 5 million cells per 10cm plate. Media was switched to BNMM supplemented with 0.02 μg/mL brain-derived neurotrophic factor (#450-02 PeproTech) + 0.02 μg/mL glial-cell-derived neurotrophic factor (#450-10 PeproTech) + 0.5 mM dbcAMP (#D0260 Sigma Aldrich). Cells were fed twice a week for three weeks. After three weeks, neurons were sorted by magnetic activated techniques to enrich the population of CD184/CD44/CD271 negative cells and plated out for experiments. All cell culture was maintained at 37C and 5% CO_2.

Purification of hiPSC-derived neurons

hiPSC-derived neurons were purified using magnetic bead sorting. Following 3 weeks of differentiation, neurons were dissociated with accutase and resuspended in Magnet Activated Cell Sorting (MACS) buffer (PBS + 0.5% bovine serum albumin [Sigma Aldrich, St Louis, MO] + 2 mM ethylenediaminetetraacetic acid [Thermo Fisher Scientific, Waltham, MA]). Following a modification of (Yuan et al., 2011), cells were incubated with PE-conjugated mouse anti-Human CD44 and mouse anti-Human CD184 antibodies (BD Biosciences, San Jose, CA) at a concentration of 5 µl/10 million cells. Following antibody incubation, cells were washed with MACS buffer and incubated with anti-PE magnetic beads (BD Biosciences, San Jose, CA) at a concentration of 25 µl/10 million cells. Bead-antibody complexes were pulled down using a rare-earth magnet, supernatants were selected, washed, and plated at an appropriate density.

DQ Red BSA assay to measure lysosomal degradation

Lysosomal proteolytic degradation was evaluated using DQ Red BSA (#D-12051; Thermo Fisher Scientific), a fluorogenic substrate for lysosomal proteases, that generates fluorescence only when enzymatically cleaved in intracellular lysosomal compartments. hiPSC-derived neurons were seeded at a density of 400,000 cells/well of a Matrigel coated 48-well plate. After 24 h, cells were washed once with DPBS, treated with complete media containing either 10 µg/ml DQ Red BSA or vehicle (PBS) and incubated for 24 h at 37 °C in a 5% CO2 incubator as described in(Marwaha and Sharma, 2017) and in(Davis et al., 2021). At the end of 24 h, cells were washed with PBS, fixed with 4% PFA and immunocytochemistry was performed as described in “Methods”. Cells were imaged using a Leica SP8 confocal microscope and all image processing was completed with ImageJ software. Cell bodies were identified by MAP2 labeling, and fluorescence intensity of DQ Red BSA was measured in regions of the images containing the MAP2 label.

Immunocytochemistry

Purified neurons were seeded at a density of 500,000 cells per well of a 24-well plate on glass coverslips coated with Matrigel. After 5 days in culture, cells were fixed in 4% paraformaldehyde (PFA, Alfa Aesar, Reston, VA) for 15 minutes. Cells were incubated in blocking buffer containing 2.5% bovine serum albumin and 0.1% Triton X-100 (Sigma Aldrich, St Louis, MO) for 30 minutes at room temperature then incubated in a primary antibody dilution in blocking buffer for 2 hours at room temperature. Cells were washed 3x with PBS + 0.1% Triton X-100 and incubated with a secondary antibody dilution in blocking buffer for 1 hour at room temperature. Cells were washed 3x in PBS and mounted on glass slides with ProLong Gold Antifade mountant (#P36930; Thermo Fisher Scientific, Waltham, MA). The following primary antibodies were used: Mouse monoclonal anti-early endosome antigen 1 (EEA1) at 1:500 (# 610456, BD Biosciences); Rabbit monoclonal anti- amyloid precursor protein (APP) at 1:500 (#32136, Abcam); Chicken polyclonal anti-microtubule-associated protein 2 (MAP2) at 1:1000 (#92434, abcam); Rabbit monoclonal anti-SORLA (#ab190684; Abcam); Rabbit polyclonal anti-VPS35 (#ab97545; Abcam);

Confocal microscopy and Image processing.

All microscopy and image processing were performed under blinded conditions. Confocal z stacks were obtained using a Nikon A1R confocal microscope with x63 and x100 plan apochromat oil immersion objectives. Image processing was performed using ImageJ software (Schindelin et al., 2012). For endosome analysis, 10-20 fields were analyzed for a total of 10-58 cells. Maximum intensity projections of confocal stacks were generated, and background was subtracted using the rolling ball algorithm. Endosome channels were enhanced using contrast limited adaptive histogram equalization algorithms (CLAHE) and masked using cell body stains. Size and intensity measurements were performed using CellProfiler software (McQuin et al., 2018). Individual puncta were identified using automated segmentation algorithms. Mean intensity of each puncta was measured and has been presented as a mean value over all puncta per field. Similarly, pixel area of each puncta was measured and has been presented as a mean area over all puncta per field. Finally, mean puncta area normalized by total cell area calculated from cell body stains is also presented. For colocalization analysis, a minimum of 10 fields of confocal z stacks were captured using the x100 plan apochromat oil immersion objective. Median filtering was used to remove noise from images and manual thresholding was applied to all images. The colocalization of APP with endocytic markers was quantified using JACOP plugin (Bolte and Cordelieres, 2006) in ImageJ and presented as Mander's correlation coefficient.

Colocalization analysis

To investigate colocalization of APP and VPS35 with early endosomes, hiPSC-derived neurons were co-labeled with either APP or VPS35 and early endosome marker EEA1, using immunocytochemistry and antibodies described in 'methods'. A minimum of 10 fields of confocal z-stack images were captured under blinded conditions using a Yokogawa W1 spinning disk confocal microscope (Nikon) and a 100X plan apochromat oil immersion objective. Median filtering was used to remove noise from images and Otsu thresholding was applied to all images. Colocalization was quantified using the JACOP plugin in Image J software and presented as Mander's correlation co-efficient . For all imaging experiments, the data were analyzed in a blinded manner.

Transferrin recycling assay

To measure recycling pathway function, we utilized transferrin recycling assay as previously described(Sakane et al., 2014) Purified neurons were seeded at 400,000 cells/well of a 24-well plate containing Matrigel coated 12 mm glass coverslips/well. After 5 DIV, cells were washed once with DMEM-F12 medium and incubated with starving medium (DMEM-F12 medium + 25 mM HEPES + 0.5% BSA) for 30 min at 37 °C in a 5% CO2 incubator to remove any residual transferrin. Thereafter, cells were pulsed with either 100 µg/ml transferrin from human serum conjugated with Alexa Fluor™ 647(#T23366; Thermo Fisher Scientific) or vehicle (PBS) in 'starving medium'. At the end of 10 min, cells were washed twice with ice-cold PBS to remove any external transferrin and stop internalization of transferrin and washed once with acid stripping buffer (25 mM citric acid + 24.5 mM sodium citrate + 280 mM sucrose + 0.01 mM Deferoxamine) to remove any membrane bound transferrin. Next, cells were either fixed in 4% PFA or 'Chase medium' (DMEM-F12 + 50 µM Deferoxamine + 20 mM HEPES + 500 µg/ml Holo-transferrin) was added for different time points. Immunocytochemistry was done using MAP2 antibody to label neurons, confocal images were captured using Leica SP8 confocal microscope under blinded conditions. Fluorescence intensity of transferrin was measured using ImageJ software.

Western Blotting

Cell lysates were run on 4%–20% Mini-PROTEAN TGX Precast Protein Gels (#4561096; Biorad) or 16.5% Criterion Tris-Tricine Gel (#3450063; BioRad) and transferred to PVDF membranes. Membranes were probed with antibodies described in the Key resources table. Imaging was performed with a BioRad ChemiDoc system and quantification was performed using ImageJ software. For Western blot analysis, hiPSC-neurons were washed with PBS and harvested in

RIPA buffer containing 1X protease and 1X phosphatase inhibitors. Total protein concentration was quantified using Pierce BCA assay kit (#23225; Thermo Fisher Scientific). Cell lysates were separated on a 4-20% Mini-PROTEAN TGX Precast Protein Gels (#4561096; Biorad). Proteins were then transferred to PVDF membranes and membranes were incubated with antibodies to Sortilin-related receptor 1 (SORLA) at 1:1000 (# ab190684; abcam); Mouse monoclonal anti-Actin (clone A4) (#MAB1501; Millipore Sigma) at 1:2000; Mouse monoclonal anti-Phospho-Tau (AT8) (#MN1020; Thermo Fisher Scientific) and Rabbit monoclonal anti-GAPDH (14C10) (#2118; Cell Signaling) and Rabbit polyclonal anti-VPS35 (#ab97545; Abcam) at 1:1000. For the PHF-Tau blots, blots were incubated overnight with PHF-1, Gift from Dr. Peter Davies, mouse 1:1000. After three washes with TBST, membranes were incubated with corresponding IRDye fluorescent secondary antibodies in intercept blocking buffer (Li-Cor) for 1h and scanned using an Odyssey Clx imaging system (Li-Cor). Full images of all Western blots in this work are shown in **Supplemental Figure 4.**

Measurement of secreted Amyloid Beta 1-40 and 1-42

Aβ peptides were measured as previously described(Young et al., 2015; Young et al., 2018). Briefly, purified neurons were seeded at a density of 200,000 cells/well of a 96-well plate and maintained in culture for 5 days. Medium and lysates were harvested from triplicate wells. To measure secreted Aβ peptides, media was run on an Aβ Triplex ELISA plate (Meso Scale Discovery #151200E-2).

Measurement of phosphorylated and total tau

Phosphorylated tau protein were measured as previously described(Young et al., 2018). Briefly, purified neurons were plated in 96 well plates at a density of 200,000 cells per well. Cell lysates and media were harvested from triplicate wells after 48 hours. To measure phosphorylated and total tau, a Phospho(Thr231)/Total Tau ELISA plate (# K15121D-2; Meso Scale Discovery) was used to assess cell lysates.

Quantification and statistical analysis

For early endosome size analysis, 3 clones of WT, 2 clones of E270K *SORL1*^{var} , 1 clone of Y141C *SORL1*^{var} , 2 clones of G511R *SORL1*^{var}, 1 clone of *SORL1*$^{+/-}$ and 2 clones of *SORL1* KO were used. 10-15 images per clones were analyzed. For experiments measuring secreted Aβ, 3 clones of WT, 2 clones of E270K *SORL1*^{var}, 1 clone of Y141C *SORL1*^{var}, 2 clones of G511R *SORL1*^{var},

1 clone of *SORL1*$^{+/-}$ and 1 clone of *SORL1* KO were used. 3 replicates per clone were analyzed for this experiment. For APP/EEA1 and VPS35/EEA1 colocalization experiments, 2 clones of WT, 2 clones of *SORL1* KO and 1 clone of *SORL1*$^{+/-}$ were used. 10 images per clone were analyzed for this experiment. For measurement of phosphorylated and total tau experiments, 2 clones of WT, 2 clones of E270K *SORL1*^{var}, 1 clone of Y141C *SORL1*^{var}, 2 clones of G511R *SORL1*^{var}, 1 clone of *SORL1*$^{+/-}$ and 2 clones of *SORL1* KO were used. 3 replicates per clone were analyzed for this experiment. For detection of tau using western blotting, 2 clones of WT and 2 clones of *SORL1* KO were used. 1-2 replicates per clone per condition were analyzed for this experiment. For early endosome size analysis with TPT-260 treatment experiments, 2 clones of WT, 2 clones of E270K *SORL1*^{var}, 1 clone of Y141C *SORL1*^{var}, 2 clones of G511R *SORL1*^{var}, 1 clone of *SORL1*$^{+/-}$ and 1 clone of *SORL1* KO were used. 15 images per clone per condition were analyzed for this experiment. For DQ-BSA assay, 1 clone of WT and 2 clones of *SORL1* KO were used and 10 images per clone per time point per condition was analyzed. For transferrin recycling assay, 2 WT clones and 2 *SORL1* KO clones were used and 10 images per clone per time point per condition were analyzed. For all imaging experiments the data was analyzed in a blinded manner. Experimental data was tested for normal distributions using the Shapiro-Wilk normality test. Normally distributed data was analyzed using parametric two-tailed unpaired t tests, one-way ANOVA tests, or two-way ANOVA tests. Non-normally distributed data was analyzed by non-parametric Kruskal-Wallis tests. Significance was defined as a value of $p > 0.05$. All statistical analysis was completed using GraphPad Prism software. Statistical details of individual experiments, including biological and technical replicate information, can be found in figure legends.

Acknowledgments

This work was supported by NIH grant R01AG062148, a BrightFocus Foundation grant (A2018656S), the WeillNeuroHub and Sponsored Research Agreements from Biogen and Retromer Therapeutics to J.E.Y. A.K. was supported by a NIH training grant (T32 AG052354). S.M is supported by a UW ADRC Development grant. Further support for this work comes from a generous gift from the Ellison Foundation (to UW). We thank all the members of the Young Laboratory as well as Dr. Tracy Young-Pearse, Dr. Scott A. Small and Dr. Gregory A. Petsko for critical comments, discussions and feedback on this work. We would like to acknowledge the UW SLU Cell Analysis Facility and the Garvey Imaging Core at the UW Institute for Stem Cell and Regenerative Medicine.

Author Contributions

Conceptualization: J.E.Y, A.K., S.M. Experimental Design: J.E.Y., A.K, and S.M. Experimental performance: A.K., S.M, R.M, C.K, P.T. Writing-Original draft: A.K. and J.E.Y. Writing-Reviewing and editing: S.M., A.K. and J.E.Y. Funding acquisition: J.E.Y, A.K, and S.M. Supervision: J.E.Y. All authors read and approved the final manuscript.

References

Andersen, O.M., Reiche, J., Schmidt, V., Gotthardt, M., Spoelgen, R., Behlke, J., von Arnim, C.A., Breiderhoff, T., Jansen, P., Wu, X.*, et al.* (2005). Neuronal sorting protein-related receptor sorLA/LR11 regulates processing of the amyloid precursor protein. Proc Natl Acad Sci U S A *102*, 13461-13466.

Andersen, O.M., Rudolph, I.M., and Willnow, T.E. (2016). Risk factor SORL1: from genetic association to functional validation in Alzheimer's disease. Acta Neuropathol *132*, 653-665.

Bhalla, A., Vetanovetz, C.P., Morel, E., Chamoun, Z., Di Paolo, G., and Small, S.A. (2012). The location and trafficking routes of the neuronal retromer and its role in amyloid precursor protein transport. Neurobiol Dis *47*, 126-134.

Caglayan, S., Takagi-Niidome, S., Liao, F., Carlo, A.S., Schmidt, V., Burgert, T., Kitago, Y., Fuchtbauer, E.M., Fuchtbauer, A., Holtzman, D.M.*, et al.* (2014). Lysosomal sorting of amyloid-beta by the SORLA receptor is impaired by a familial Alzheimer's disease mutation. Science translational medicine *6*, 223ra220.

Cataldo, A.M., Hamilton, D.J., Barnett, J.L., Paskevich, P.A., and Nixon, R.A. (1996). Properties of the endosomal-lysosomal system in the human central nervous system: disturbances mark most neurons in populations at risk to degenerate in Alzheimer's disease. J Neurosci *16*, 186-199.

Cataldo, A.M., Petanceska, S., Terio, N.B., Peterhoff, C.M., Durham, R., Mercken, M., Mehta, P.D., Buxbaum, J., Haroutunian, V., and Nixon, R.A. (2004). Abeta localization in abnormal endosomes: association with earliest Abeta elevations in AD and Down syndrome. Neurobiol Aging *25*, 1263-1272.

Cataldo, A.M., Peterhoff, C.M., Troncoso, J.C., Gomez-Isla, T., Hyman, B.T., and Nixon, R.A. (2000). Endocytic pathway abnormalities precede amyloid beta deposition in sporadic Alzheimer's disease and Down syndrome: differential effects of APOE genotype and presenilin mutations. Am J Pathol *157*, 277-286.

Das, U., Wang, L., Ganguly, A., Saikia, J.M., Wagner, S.L., Koo, E.H., and Roy, S. (2016). Visualizing APP and BACE-1 approximation in neurons yields insight into the amyloidogenic pathway. Nat Neurosci *19*, 55-64.

Dodson, S.E., Andersen, O.M., Karmali, V., Fritz, J.J., Cheng, D., Peng, J., Levey, A.I., Willnow, T.E., and Lah, J.J. (2008). Loss of LR11/SORLA enhances early pathology in a mouse model of amyloidosis: evidence for a proximal role in Alzheimer's disease. J Neurosci *28*, 12877-12886.

Fjorback, A.W., Seaman, M., Gustafsen, C., Mehmedbasic, A., Gokool, S., Wu, C., Militz, D., Schmidt, V., Madsen, P., Nyengaard, J.R.*, et al.* (2012). Retromer binds the FANSHY sorting motif in SorLA to regulate amyloid precursor protein sorting and processing. J Neurosci *32*, 1467-1480.

Holstege, H., van der Lee, S.J., Hulsman, M., Wong, T.H., van Rooij, J.G., Weiss, M., Louwersheimer, E., Wolters, F.J., Amin, N., Uitterlinden, A.G.*, et al.* (2017). Characterization of pathogenic SORL1 genetic variants for association with Alzheimer's disease: a clinical interpretation strategy. Eur J Hum Genet *25*, 973-981.
Hung, C., Tuck, E., Stubbs, V., van der Lee, S.J., Aalfs, C., van Spaendonk, R., Scheltens, P., Hardy, J., Holstege, H., and Livesey, F.J. (2021). SORL1 deficiency in human excitatory neurons causes APP-dependent defects in the endolysosome-autophagy network. Cell Rep *35*, 109259.
Karch, C.M., and Goate, A.M. (2015). Alzheimer's disease risk genes and mechanisms of disease pathogenesis. Biol Psychiatry *77*, 43-51.
Knupp, A., Mishra, S., Martinez, R., Braggin, J.E., Szabo, M., Kinoshita, C., Hailey, D.W., Small, S.A., Jayadev, S., and Young, J.E. (2020). Depletion of the AD Risk Gene SORL1 Selectively Impairs Neuronal Endosomal Traffic Independent of Amyloidogenic APP Processing. Cell Rep *31*, 107719.
Kwart, D., Gregg, A., Scheckel, C., Murphy, E.A., Paquet, D., Duffield, M., Fak, J., Olsen, O., Darnell, R.B., and Tessier-Lavigne, M. (2019). A Large Panel of Isogenic APP and PSEN1 Mutant Human iPSC Neurons Reveals Shared Endosomal Abnormalities Mediated by APP beta-CTFs, Not Abeta. Neuron *104*, 256-270 e255.
Le Guennec, K., Tubeuf, H., Hannequin, D., Wallon, D., Quenez, O., Rousseau, S., Richard, A.C., Deleuze, J.F., Boland, A., Frebourg, T.*, et al.* (2018). Biallelic Loss of Function of SORL1 in an Early Onset Alzheimer's Disease Patient. J Alzheimers Dis *62*, 821-831.
Levy, S., Sutton, G., Ng, P.C., Feuk, L., Halpern, A.L., Walenz, B.P., Axelrod, N., Huang, J., Kirkness, E.F., Denisov, G.*, et al.* (2007). The diploid genome sequence of an individual human. PLoS Biol *5*, e254.
Li, J.G., Chiu, J., Ramanjulu, M., Blass, B.E., and Pratico, D. (2020). A pharmacological chaperone improves memory by reducing Abeta and tau neuropathology in a mouse model with plaques and tangles. Mol Neurodegener *15*, 1.
Marwaha, R., and Sharma, M. (2017). DQ-Red BSA Trafficking Assay in Cultured Cells to Assess Cargo Delivery to Lysosomes. Bio Protoc *7*.
Mecozzi, V.J., Berman, D.E., Simoes, S., Vetanovetz, C., Awal, M.R., Patel, V.M., Schneider, R.T., Petsko, G.A., Ringe, D., and Small, S.A. (2014). Pharmacological chaperones stabilize retromer to limit APP processing. Nature chemical biology *10*, 443-449.
Mishra, S., Knupp, A., Szabo, M.P., Williams, C.A., Kinoshita, C., Hailey, D.W., Wang, Y., Andersen, O.M., and Young, J.E. (2022). The Alzheimer's gene SORL1 is a regulator of endosomal traffic and recycling in human neurons. Cell Mol Life Sci *79*, 162.
Ouellette, S.P., and Carabeo, R.A. (2010). A Functional Slow Recycling Pathway of Transferrin is Required for Growth of Chlamydia. Front Microbiol *1*, 112.
Pottier, C., Hannequin, D., Coutant, S., Rovelet-Lecrux, A., Wallon, D., Rousseau, S., Legallic, S., Paquet, C., Bombois, S., Pariente, J.*, et al.* (2012). High frequency of potentially pathogenic SORL1 mutations in autosomal dominant early-onset Alzheimer disease. Molecular psychiatry *17*, 875-879.
Rogaeva, E., Meng, Y., Lee, J.H., Gu, Y., Kawarai, T., Zou, F., Katayama, T., Baldwin, C.T., Cheng, R., Hasegawa, H.*, et al.* (2007). The neuronal sortilin-related receptor SORL1 is genetically associated with Alzheimer disease. Nat Genet *39*, 168-177.

Rose, S.E., Frankowski, H., Knupp, A., Berry, B.J., Martinez, R., Dinh, S.Q., Bruner, L.T., Willis, S.L., Crane, P.K., Larson, E.B.*, et al.* (2018). Leptomeninges-Derived Induced Pluripotent Stem Cells and Directly Converted Neurons From Autopsy Cases With Varying Neuropathologic Backgrounds. J Neuropathol Exp Neurol.
Scheltens, P., De Strooper, B., Kivipelto, M., Holstege, H., Chetelat, G., Teunissen, C.E., Cummings, J., and van der Flier, W.M. (2021). Alzheimer's disease. Lancet *397*, 1577-1590.
Simoes, S., Guo, J., Buitrago, L., Qureshi, Y.H., Feng, X., Kothiya, M., Cortes, E., Patel, V., Kannan, S., Kim, Y.H.*, et al.* (2021). Alzheimer's vulnerable brain region relies on a distinct retromer core dedicated to endosomal recycling. Cell Rep *37*, 110182.
Small, S.A., Kent, K., Pierce, A., Leung, C., Kang, M.S., Okada, H., Honig, L., Vonsattel, J.P., and Kim, T.W. (2005). Model-guided microarray implicates the retromer complex in Alzheimer's disease. Annals of neurology *58*, 909-919.
Small, S.A., Simoes-Spassov, S., Mayeux, R., and Petsko, G.A. (2017). Endosomal Traffic Jams Represent a Pathogenic Hub and Therapeutic Target in Alzheimer's Disease. Trends Neurosci *40*, 592-602.
Sonnichsen, B., De Renzis, S., Nielsen, E., Rietdorf, J., and Zerial, M. (2000). Distinct membrane domains on endosomes in the recycling pathway visualized by multicolor imaging of Rab4, Rab5, and Rab11. J Cell Biol *149*, 901-914.
Tan, J.Z.A., and Gleeson, P.A. (2019). The role of membrane trafficking in the processing of amyloid precursor protein and production of amyloid peptides in Alzheimer's disease. Biochim Biophys Acta Biomembr *1861*, 697-712.
Tang, M., Harrison, J., Deaton, C.A., and Johnson, G.V.W. (2019). Tau Clearance Mechanisms. Adv Exp Med Biol *1184*, 57-68.
Toh, W.H., Chia, P.Z.C., Hossain, M.I., and Gleeson, P.A. (2018). GGA1 regulates signal-dependent sorting of BACE1 to recycling endosomes, which moderates Abeta production. Mol Biol Cell *29*, 191-208.
Vardarajan, B.N., Zhang, Y., Lee, J.H., Cheng, R., Bohm, C., Ghani, M., Reitz, C., Reyes-Dumeyer, D., Shen, Y., Rogaeva, E.*, et al.* (2014). Coding mutations in SORL1 and Alzheimer's disease. Annals of neurology.
Young, J.E., Boulanger-Weill, J., Williams, D.A., Woodruff, G., Buen, F., Revilla, A.C., Herrera, C., Israel, M.A., Yuan, S.H., Edland, S.D.*, et al.* (2015). Elucidating Molecular Phenotypes Caused by the SORL1 Alzheimer's Disease Genetic Risk Factor Using Human Induced Pluripotent Stem Cells. Cell stem cell *16*, 373-385.
Young, J.E., Fong, L.K., Frankowski, H., Petsko, G.A., Small, S.A., and Goldstein, L.S.B. (2018). Stabilizing the Retromer Complex in a Human Stem Cell Model of Alzheimer's Disease Reduces TAU Phosphorylation Independently of Amyloid Precursor Protein. Stem Cell Reports *10*, 1046-1058.
Yuan, S.H., Martin, J., Elia, J., Flippin, J., Paramban, R.I., Hefferan, M.P., Vidal, J.G., Mu, Y., Killian, R.L., Israel, M.A.*, et al.* (2011). Cell-surface marker signatures for the isolation of neural stem cells, glia and neurons derived from human pluripotent stem cells. PLoS One *6*, e17540.

FIGURE LEGENDS

Figure 1. **SORL1$^{+/-}$ and SORL1^{Var} hiPSC-derived neurons have swollen early endosomes and increased Aβ secretion (A)** Representative immunofluorescent images of WT, heterozygous *SORL1^{Var}*, *SORL1$^{+/-}$*, and *SORL1* KO hiPSC-derived neurons. Neurons are stained with EEA1 (green) to mark early endosomes, MAP2 (red) to mark cell bodies, and DAPI (blue) to mark nuclei. Scale bar: 5 µm. **(B)** The size of EEA puncta is larger in *SORL1*^{Var}, *SORL1$^{+/-}$*, and *SORL1*KO neurons, indicated by asterisks. *SORL1*KO neurons have the largest endosome size, the size of *SORL1*^{Var} and *SORL1$^{+/-}$* neurons is different than *SORL1*KO, indicated by hash marks. **(C-D)** Heterozygous *SORL1*^{Var}, *SORL1$^{+/-,}$* and *SORL1*KO hiPSC-derived neurons secrete significantly increased levels of **(C)**Aβ_{40} and **(D)**Aβ_{42} as compared to WT controls. Also, *SORL1* KO neurons secrete significantly increased levels of Aβ_{40} and Aβ_{42} as compared to *SORL1*^{Var} and *SORL1$^{+/-}$* hiPSC-derived neurons. Asterisks indicate significance relative to WT hiPSC-derived neurons and hashmarks indicate significance relative to *SORL1* KO hiPSC-derived neurons. For imaging experiments, 10-15 images and 1-3 clones were analyzed per genotype. For Aβ secretion experiments, 1-3 clones and 3 replicates per clone per genotype were used. Data represented as mean ± SD. Data was analyzed using parametric one-way ANOVA. Significance was defined as a value of *$p < 0.05$, **$p < 0.01$, ***$p < 0.001$, and ****$p < 0.0001$.

Figure 2**. Retromer enhancement with TPT-260 reduces AD pathological phenotypes**
(A) Representative immunofluorescent images of TPT-260 and DMSO-treated WT, heterozygous *SORL1^{Var}*, *SORL1$^{+/-}$* and *SORL1* KO hiPSC-derived neurons. Neurons are stained with EEA1 (green) to mark early endosomes, MAP2 (red) to mark cell bodies, and DAPI (blue) to mark nuclei. Scale bar: 5 µm. **(B)** All TPT-260 treated neurons have early endosomes that are smaller than the DMSO-treated controls. While TPT-260 treatment had no effect on endosome size in WT neurons, it significantly reduced endosome size in *SORL1*^{Var}, *SORL1$^{+/-}$*, and *SORL1*KO neurons compared with DMSO treatment (indicated by asterisks). The reduction of endosomes size in SORI1KO was significantly different from *SORL1*^{Var} and *SORL1$^{+/-}$* neurons (indicated by hashmarks). N=10-20 images analyzed per genotype. Data represented as mean ± SD. **(C-D)** Levels of secreted Aβ 1-40 **(C)** and Aβ 1-42 **(D)** are reduced with TPT-260 treatment in all genotypes except secreted Aβ 1-42 in *SORL1* KO neurons, as compared to their respective DMSO treated counterparts. The % decrease in Aβ 1-40 and Aβ 1-42 levels of TPT-260 treated cells respective to DMSO controls, is significantly higher in heterozygous *SORL1^{Var}* and *SORL1$^{+/-}$* neurons as compared to *SORL1* KO neurons. Asterisks indicate significance relative to respective DMSO treated counterparts and hashmarks indicate significance relative to TPT-260 treated *SORL1* KO hiPSC-derived neurons. Data is represented as secreted Aβ levels normalized to the

DMSO controls. For all experiments, 1-3 clones and 3 replicates per clone per genotype were used. Data represented as mean ±SD. (**E-G**) Tau phosphorylation on three epitopes was examined in response to TPT-260 treatment. **(E)** Thr 231 epitope levels, as measured by ELISA assay, is reduced in all the genotypes treated with TPT-260 relative to WT DMSO controls **(F)** The PHF-1 (Ser396/Ser404) and the **(G)** AT8(Ser202/Thr305) epitopes as measured by western blot is decreased in TPT-260 treated *SORL1* KO hiPSC-derived neurons relative to WT DMSO controls. 1-3 clones were analyzed per genotype. Data represented as mean ± SD. Normally distributed data was analyzed using parametric two-way ANOVA. 1-3 clones were analyzed per genotype. Significance was defined as a value of *p < 0.05, **p < 0.01, ***p < 0.001, and ****p < 0.0001. ns=not significant. * indicates statistical difference as compared to WT and # indicates statistical difference as compared to *SORL1* KO.

Figure 3. **TPT-260 treatment reduces localization of APP and VPS35 in early endosomes. (A-B)** Co-localization of VPS35 (green) with EEA1 (red) is not different between WT and *SORL1*KO neurons treated with TPT-260 (white arrows). **(C-D)** Co-localization of APP (green) with EEA1 (red) co-localization is increased in *SORL1*KO neurons treated with TPT-260 (white arrows). In *SORL1*$^{+/-}$ neurons, APPP/EEA1 colocalization with TPT-260 treatment is not different than WT neurons treated with TPT-260 (white arrows). Scale bar: 5 µm. For co-localization analysis, 10-15 images per clones and 1-3 clones were analyzed per genotype. Data represented as mean ± SD. Data was analyzed using parametric one-way ANOVA. Significance was defined as a value of *p < 0.05, **p < 0.01, ***p < 0.001, and ****p < 0.0001.

Figure 4. **Retromer enhancement with TPT-260 enhances lysosomal degradation and endosomal recycling in *SORL1* KO neurons. (A-B)** TPT-260 rescues lysosomal trafficking and degradation of DQ-Red BSA. **(A)** Representative images of WT and SORL1 KO neurons treated with DQ-Red-BSA for 24 hours. **(B)**TPT-260 rescues lysosomal degradation as evidenced by increased fluorescence intensity of DQ-Red BSA after 24 hrs in TPT-260 treated *SORL1* KO hiPSC-derived neurons as compared to its DMSO treated counterpart. There is no difference between DMSO treated and TPT-260 treated WT hiPSC-derived neurons**.** Neurons are labeled with DQ-Red-BSA (red), MAP2 (cell bodies-green) and DAPI (nuclei-blue). Scale bar: 5 µm **(C-D)** TPT-260 treatment partially rescues endosomal recycling as measured by the transferrin assay at 10 min and 40 minutes of transferrin recycling in *SORL1* KO hiPSC-derived neurons. While TPT-260 treatment in *SORL1*KO neurons (orange line/orange triangles) leads to faster transferrin recycling in SORL1KO neurons compared with DMSO (red line/red triangles), after 40 minutes

transferrin recycling in the SORL1KO TPT-260 treated neurons (orange line/orange triangles) is still different than WT recycling (black and gray lines/black and gray circles). Asterisks indicate a statistical difference between WT DMSO and *SORL1*KO DMSO; hashmarks indicate a statistical difference between *SORL1*KO+TPT-260 and WT+DMSO and WT+TPT-260. Neurons are labeled with transferrin-647 (purple), MAP2 (cell bodies-green) and DAPI (nuclei-blue). Scale bar: 5 µm. Data represented as transferrin intensity normalized to time 0. 10 images per clone per genotype per timepoint were analyzed. 1-3 clones per genotype were analyzed. Data represented as mean +/- SD. Data represented as mean ± SD. Normally distributed data was analyzed using parametric two-way ANOVA. Significance was defined as a value of *$p < 0.05$, **$p < 0.01$, ***$p < 0.001$, and ****$p < 0.0001$. ns= not significant.

Supplemental Figure Legends

Supplemental Figure 1. Characterization of *SORL1*^{Var} and *SORL1*$^{+/-}$ cell lines.

A) Sanger sequencing showing heterozygous base-pair change for each SORL1^{Var} hiPSC line. **B)** Representative Western blots showing that SORL1^{Var} hiPSCs have equivalent levels of SORLA protein expression to WT. **C)** Quantification of Western blots. **D)** Sanger sequencing showing heterozygous insertion/deletion (indel) leading to SORL1$^{+/-}$ hiPSC line. **E)** Representative Western blots showing that SORL1$^{+/-}$ hiPSCs have less SORLA protein expression than WT hiPSCs. **F)** Quantification of Western blots.

Supplemental Figure 2. Phospho-tau levels in *SORL1*KO, *SORL1*^{Var} and *SORL1*$^{+/-}$ neurons.

A-C) No significant change in phospho-tau at two epitopes was detected in *SORL1*KO, *SORL1*^{Var}, or *SORL1*$^{+/-}$ neurons. **A)** Representative Western blot of PHF-1 phospho-tau epitope. **B)** Quantification of Western blot. **C)** ELISA assay of Thr 231 phospho-Tau epitope.

Supplemental Figure 3. TPT-260 treatment increases VPS35 levels and is not cytotoxic.

A) Representative Western blots showing VPS35 protein after TPT-260 treatment in *SORL1*KO, *SORL1*^{Var}, or *SORL1*$^{+/-}$ neurons. **B)** Quantification of Western blots. **C)** LDH cytotoxicity assay shows no significant increase in cell death after TPT-260 treatment in *SORL1*KO, *SORL1*^{Var}, or *SORL1*$^{+/-}$ neurons.

Figure 1.

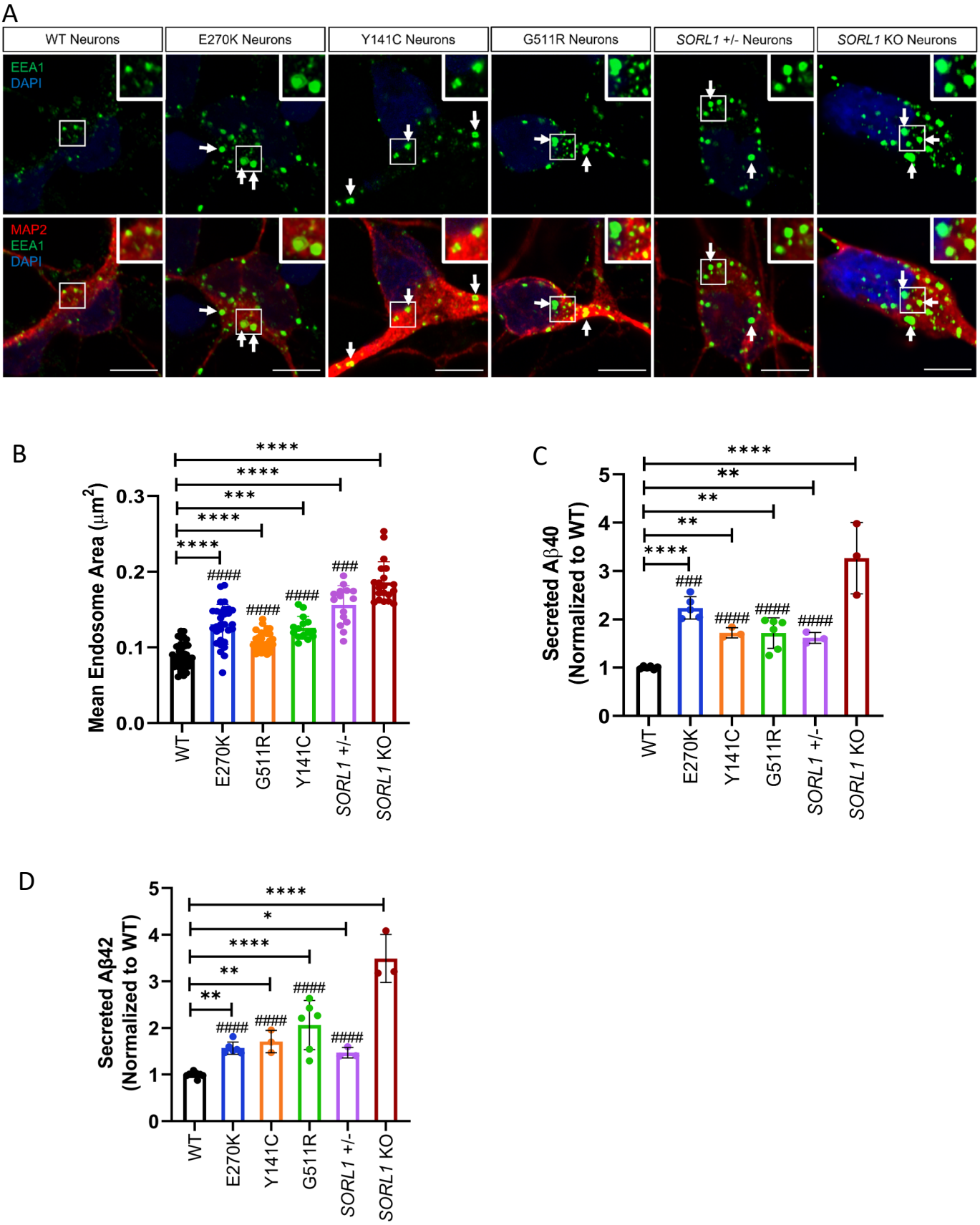
A
WT Neurons
E270K Neurons
Y141C Neurons
G511R Neurons
SORL1 +/- Neurons
SORL1 KO Neurons
EEA1
DAPI
MAP2
EEA1
DAPI
B
Mean Endosome Area (μm²)
0.0
0.1
0.2
0.3
****
****
***
****
****
####
####
####
###
WT
E270K
G511R
Y141C
SORL1 +/-
SORL1 KO
C
Secreted Aβ40 (Normalized to WT)
0
1
2
3
4
5
****
**
**
**
****
###
####
####
####
WT
E270K
Y141C
G511R
SORL1 +/-
SORL1 KO
D
Secreted Aβ42 (Normalized to WT)
0
1
2
3
4
5
****
*
****
**
**
####
####
####
####
WT
E270K
Y141C
G511R
SORL1 +/-
SORL1 KO

Figure 2.

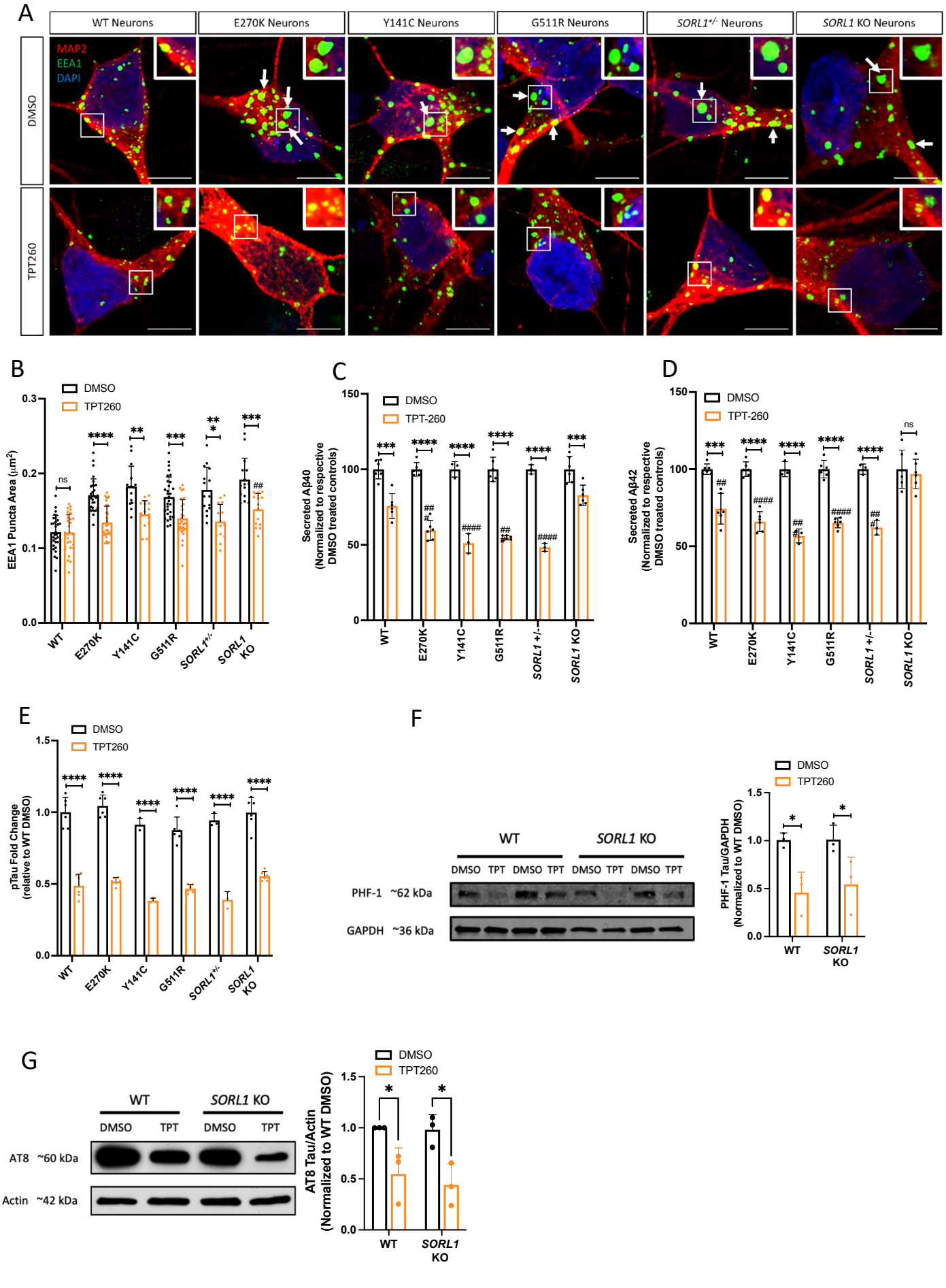
A
WT Neurons
E270K Neurons
Y141C Neurons
G511R Neurons
SORL1+/- Neurons
SORL1 KO Neurons
MAP2
EEA1
DAPI
DMSO
TPT260
B
EEA1 Puncta Area (μm²)
C
Secreted Aβ40 (Normalized to respective DMSO treated controls)
D
Secreted Aβ42 (Normalized to respective DMSO treated controls)
TPT-260
E
pTau Fold Change (relative to WT DMSO)
F
WT
SORL1 KO
DMSO TPT DMSO TPT DMSO TPT DMSO TPT
PHF-1 ~62 kDa
GAPDH ~36 kDa
PHF-1 Tau/GAPDH (Normalized to WT DMSO)
G
AT8 ~60 kDa
Actin ~42 kDa
AT8 Tau/Actin (Normalized to WT DMSO)

Figure 3.

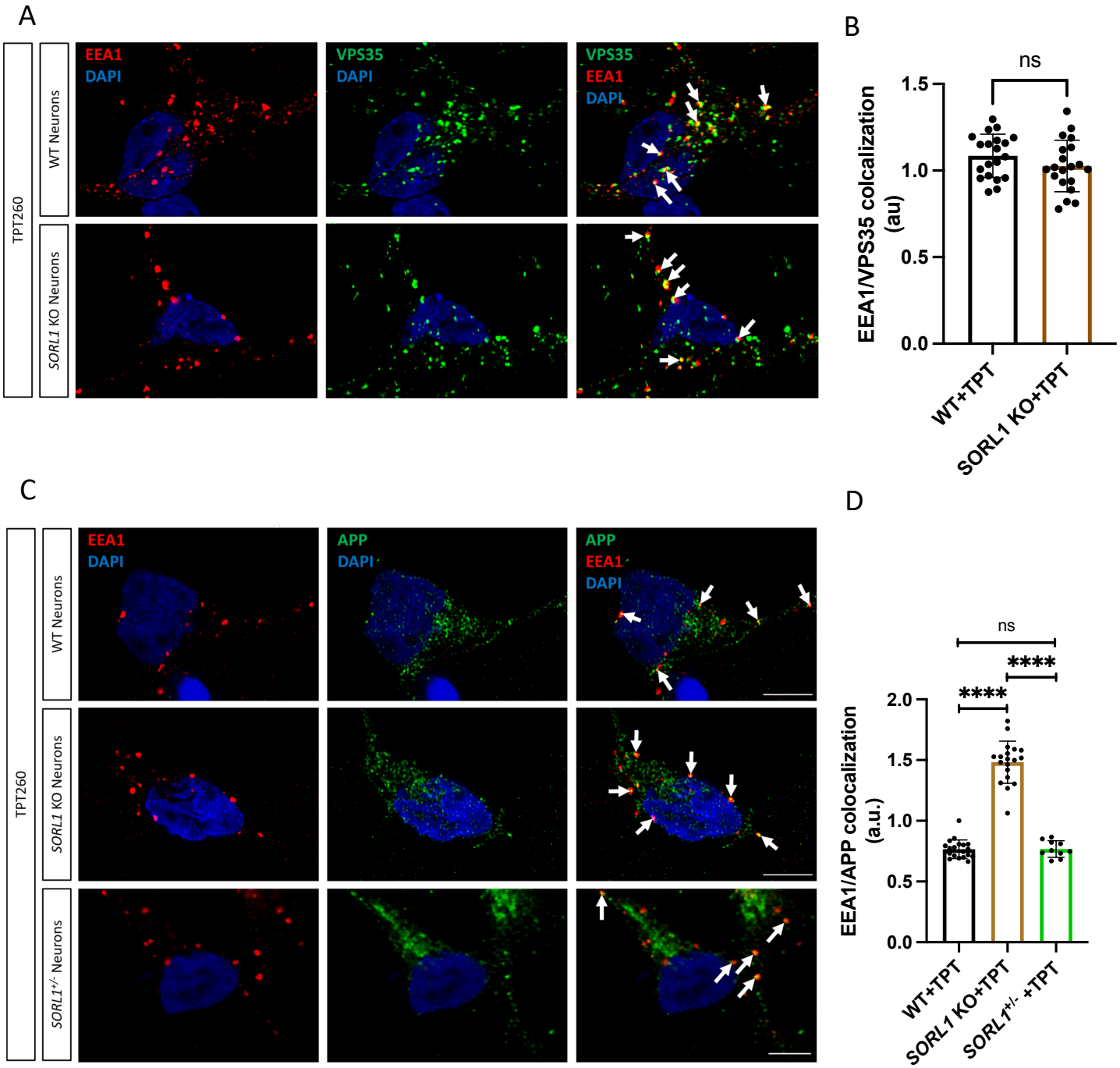
A
TPT260
WT Neurons
SORL1 KO Neurons
EEA1
DAPI
VPS35
DAPI
VPS35
EEA1
DAPI
B
ns
EEA1/VPS35 colcalization (au)
1.5
1.0
0.5
0.0
WT+TPT
SORL1 KO+TPT
C
TPT260
WT Neurons
SORL1 KO Neurons
SORL1+/- Neurons
EEA1
DAPI
APP
DAPI
APP
EEA1
DAPI
D
ns
****
****
EEA1/APP colocalization (a.u.)
2.0
1.5
1.0
0.5
0.0
WT+TPT
SORL1 KO+TPT
SORL1+/- +TPT

Figure 4.

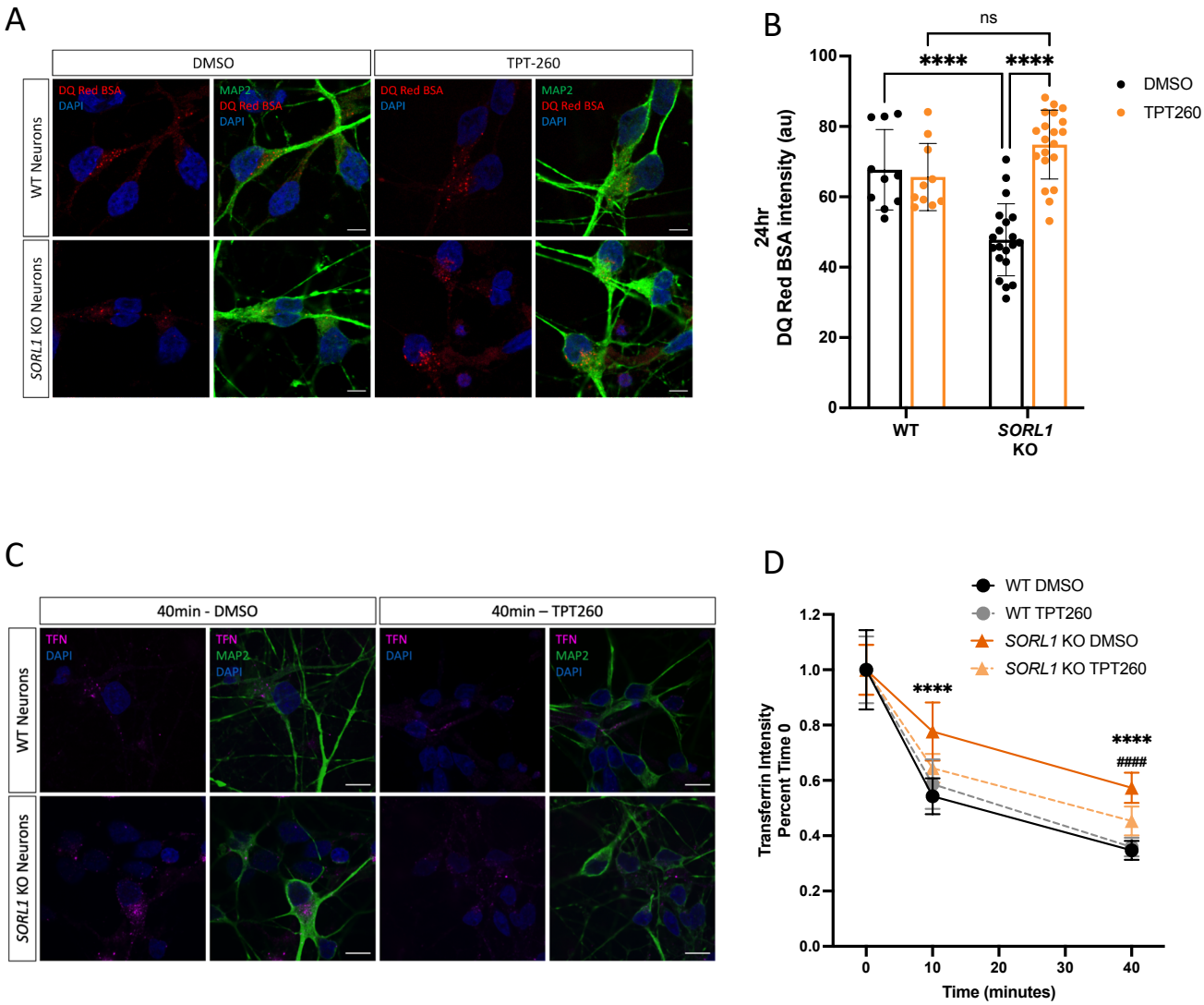
A
DMSO
TPT-260
WT Neurons
SORL1 KO Neurons
DQ Red BSA
DAPI
MAP2
B
ns
****
****
DMSO
TPT260
24hr
DQ Red BSA intensity (au)
WT
SORL1
KO
C
40min - DMSO
40min – TPT260
TFN
MAP2
D
WT DMSO
WT TPT260
SORL1 KO DMSO
SORL1 KO TPT260
Transferrin Intensity
Percent Time 0
Time (minutes)
####

Supplemental Figure 1.

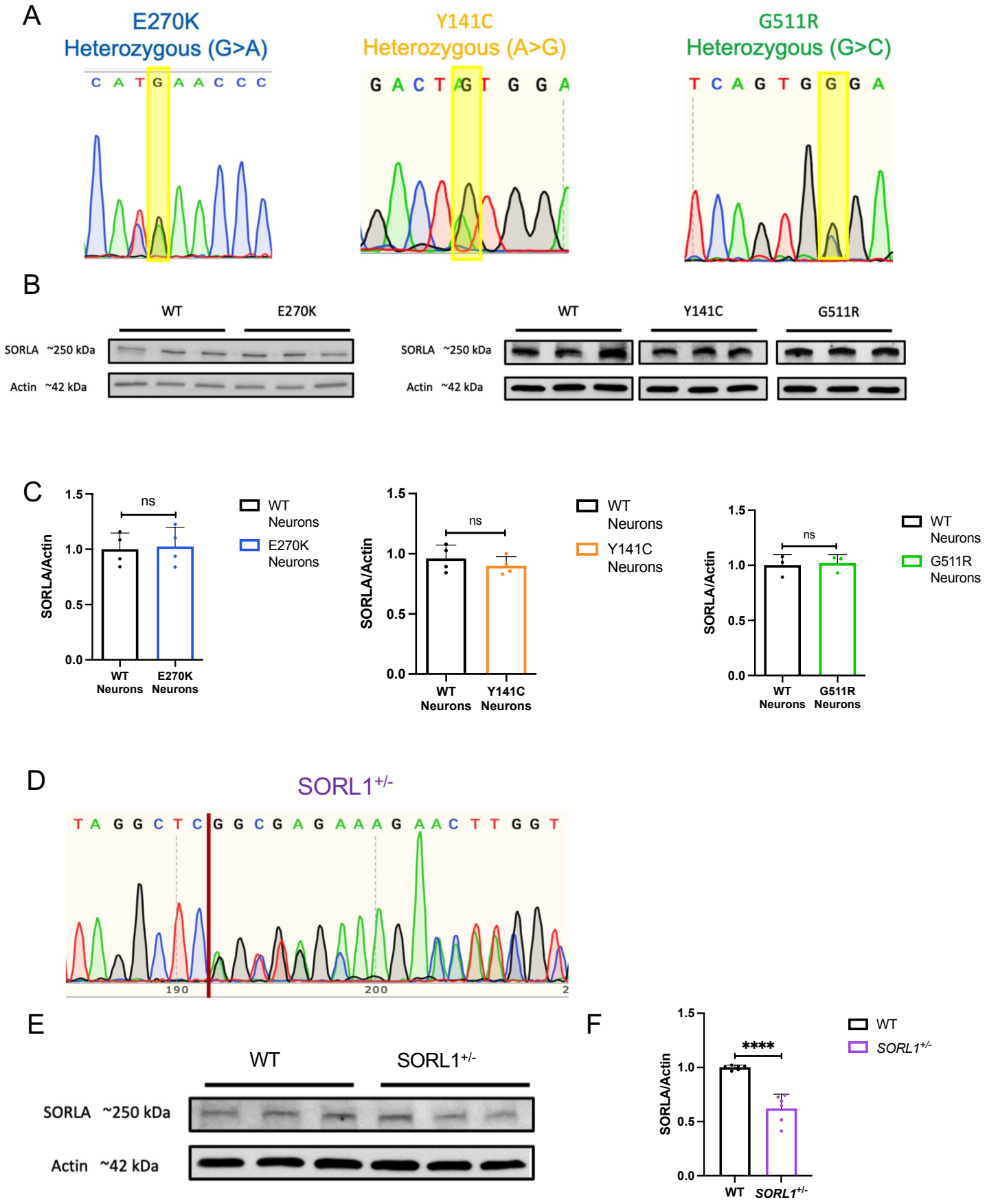

Supplemental Figure 2.

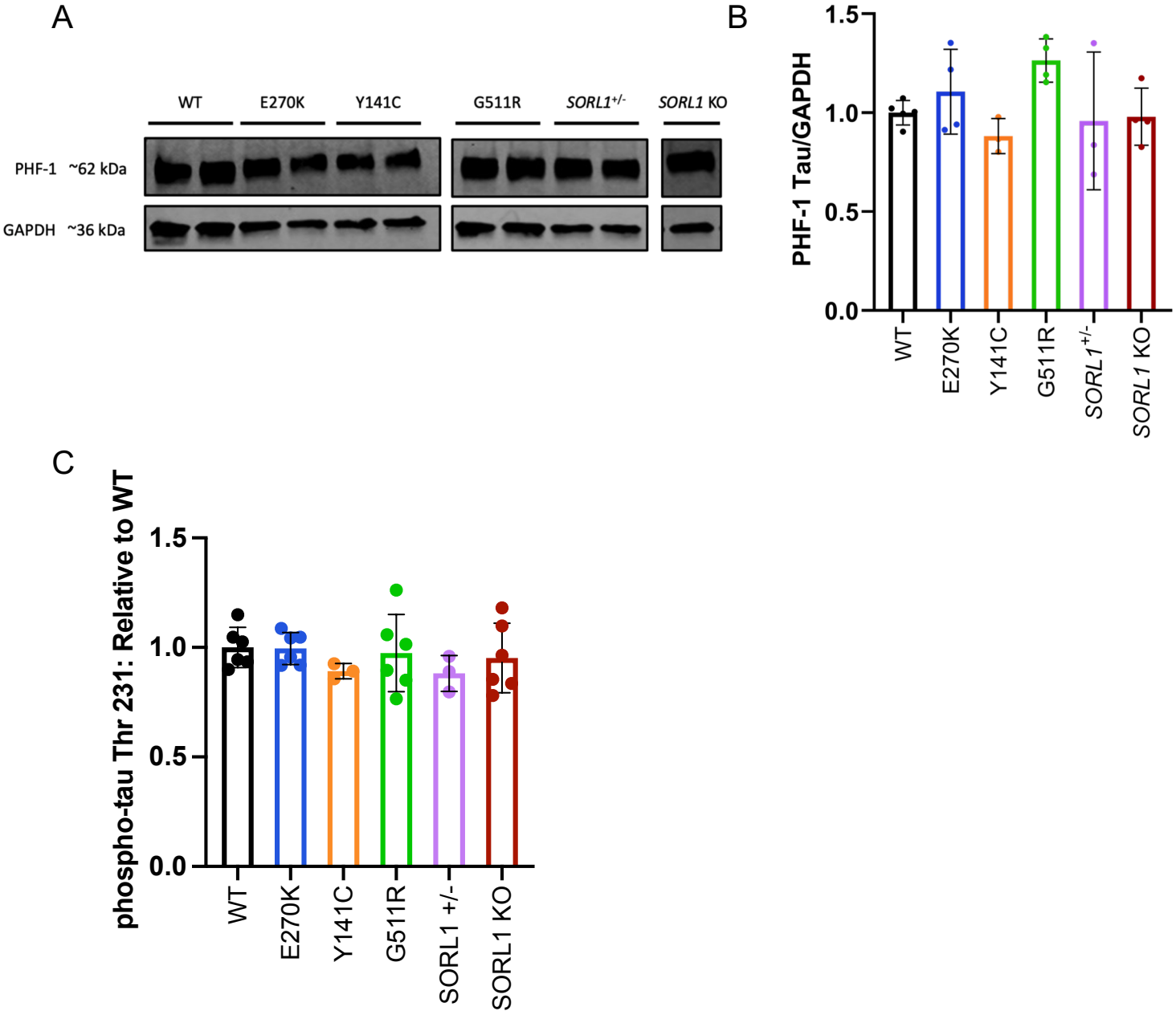
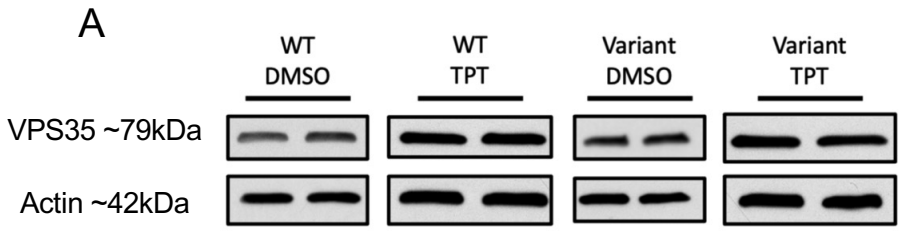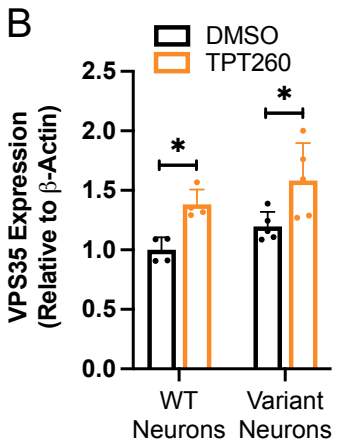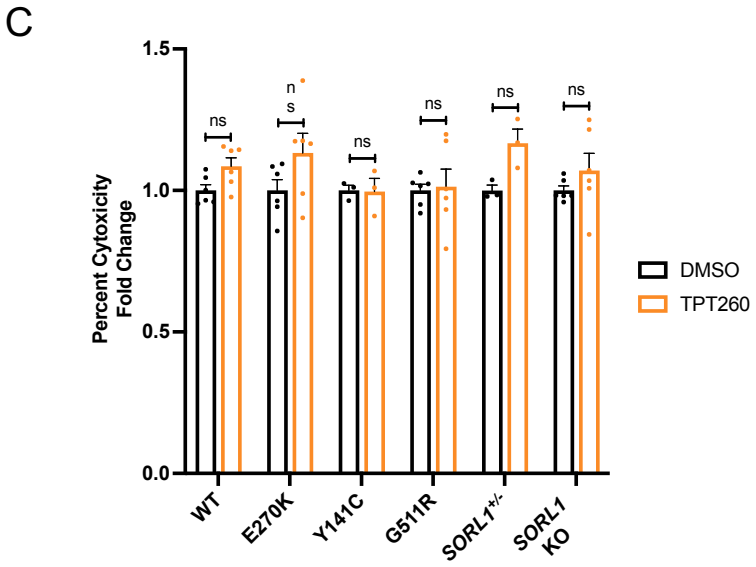
Supplemental Figure 3